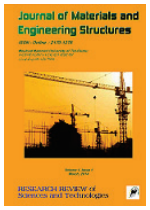

Journal of Materials and Engineering Structures

Research Paper

The effect of paste volume and concrete properties on size independent fracture energy

Ghoson Danhash [a]*, ***Mayada Kousa*** [a], ***George Wardeh*** [b]

[a] *Damascus university, Syrian Arab Republic.*

[b] *University of Cergy-Pontoise, France.*

ARTICLE INFO

Article history :

Received : 20 February 2014

Revised : 14 July 2014

Accepted : 20 July 2014

Keywords:

concrete

fracture energy

inverse analysis

paste volume

ABSTRACT

Post peak tensile behavior of concrete, softening, can be described using bi-linear curve. The area under this curve is the fracture energy G_F which is necessary for the structural design. RILEM presented a recommendation for calculating G_F but unfortunately the obtained value is size dependent. In this paper a large number of experimental Forces – Crack Mouth Opening Displacement (F-CMOD) curves, obtained from three points bending tests, were analyzed through an inverse analysis procedure to obtain the size independent fracture parameters.

The effect of compressive strength, aggregate size, and paste volume on the fracture behavior of concrete were studied and compared with the empirical formulas found in the literature.

A new empirical relationship for the prediction of size independent fracture energy of concrete from compressive strength, aggregate size and paste volume was proposed. It is shown that the proposed model can predict the size independent fracture energy with a good accuracy.

1 Introduction

Quasi brittle materials like plain concrete have softening behavior which is the decrease in tensile stress with the increase in crack opening. The relation between stress and crack tip opening is called softening curve, $(\boldsymbol{\sigma - w})$, and the area under this curve is fracture energy which is important for structural design.

Softening curve can be found from tension test which is not easy to be performed, and the alternative test to specify this softening curve is three points bending test according to RILEM recommendations [3].

The tensile fracture behavior can be described through the fictitious crack model developed by Hillerborg et al. [1]. In general, σ-w relationship is non-linear and it is accepted that a bilinear curve can describe the real fracture behavior in

* *Ghoson DANHASH. Tel.: +963955563137.*
E-mail address: ghosoun.d@gmail.com

concrete (see Fig.A.1) [2]. The main parameters of the fictitious crack model are: the tensile strength Ft, the elastic modulus E, σ-w curve and the fracture energy G_F. Fracture parameters are the fracture energy G_F, the characteristic length L_{ch} of concrete, which depends on (E, F_t, G_F), and the parameters of softening curve (a_1, a_2, b_2), see Fig.A.1.

RILEM has put recommendations for calculating G_F from three points bending test on notched beams [3]. From this test two curves are obtained, the first one is Force – Crack Mouth Opening Displacement curve (F-CMOD) and the second one is Force-Deflection curve. Fracture energy due to RILEM is taken equal to the area under the Force-Deflection curve divided by the area of ligament. Unfortunately this method suffers from size effect problem where the results are highly influenced by specimens size and notch's height [4]. As G_F is considered as a material property, so it is supposed to be the same value whatever is the size of the specimen, this means that it should be size independent.

Size dependency problem has been solved later by inverse analysis procedure with finite element method [2]. Inverse analysis procedure calculates the size independent fracture parameters by comparing the experimental F-CMOD curve derived from three points bending test with the numerical one.

Finite element method was the only way to calculate F-CMOD curve until Ulfkjaer [5] has presented an analytical model depending on linear softening. Olesen [6] adopted Ulfkjaer analytical model but he used bilinear softening instead of linear one. Ostergaard has used later this analytical model of Olesen and developed an inverse algorithm to optimize the fracture parameters of concrete [7]. In this research the inverse analysis procedure using the analytical bilinear model of Olesen has been adopted in order to obtain the size independent fracture energy G_F and bilinear curve's parameters for several types of concrete (Appendix A.4). Using this procedure a large experimental data from three point bending test on notched beams has been analyzed to get size independent fracture parameters. Using this size independent fracture parameters, the relation between fracture parameters and material properties of concrete has been studied.

Several empirical relationships have been proposed in the literature to predict fracture energy G_F in concrete depending on compressive strength F'c, maximum aggregates size d_{max} , and some of them added water to cement ratio [8-10]. Those empirical relations have been proposed using size dependent G_F. The present work focuses on the optimization of a new relationship that is based on the obtained size independent G_F. In this relation a new parameter which is paste volume has been used for the first time in predicting G_F with another two parameters which are compressive strength F'c and maximum aggregate size d_{max}.

2 Experimental procedure and specimens.

2.1 Materials

2.1.1 Materials of the research:

Three different concretes were prepared using normal Portland cement with maximum aggregate size of 20 [mm]. The beams were cured in water at room temperature.

2.1.2 Materials from literature:

Some concretes from other researches were chosen for enriching the database. The concretes from literature are: seven different concretes for Zhao [11], one for Roesler [12], one for Einsfield [13], three for Casuccio [14], and eight for Zhang [15]. Maximum aggregate size varies between 10-80 mm for specifying the effect of aggregate size on fracture parameters. Moreover, the paste volume (volume of water + powder in 1 m^3) for each mix was calculated in order to evaluate its influence on fracture energy. For all mixes, the density of cement was equal to 3100 kg/m^3 and density of fly ash was fixed to 2200 kg/m^3. The compositions of the studied materials are described in Table 1.

2.2 Specimens

Beams of different sizes were cast for bending test where central notches have been milled with different lengths. The ratio a_0/H (notch's length/ beam height) varies from 0.1 to 0.5 so we can specify its effect on fracture parameters. Cylindrical specimens were also casted and tested to determine compressive strength, splitting strength and elastic modulus. The dimensions of the studied beams are shown in Table 2.

2.3 Testing procedure

Three points bending tests were carried out on notched beams, according to RILEM recommendations [3], using testing machines controlled in displacement mode with a speed rate of 1 mm/sec. Deflection was recorded using LVDT (Linear Variable Differential Transformer), while the crack opening displacement was recorded by clip-gauge attached to knife-edges that was installed at the bottom of tested beams. Finally experimental Force-CMOD curves are obtained for analyzing them with the inverse analysis procedure to get size independent fracture parameters.

Table 1: Mix proportions of the studied concretes.

Mix	Cement [Kg/m^3]	Gravel [Kg/m^3]	D_{max} [mm]	Sand [Kg/m^3]	Water [Kg/m^3]	W.R [Kg/m^3]	Fly ash	W/C	A.E%	Paste volume
C1	350	1065	20	970	164	1.89	-	0.47	-	0.28
C2	400	1081	20	777	130	1.9	-	0.32	-	0.26
C3	400	1081	20	777	160	-	-	0.4	-	0.29
SG1 [11]	196	1090	10	869	140	1.68	84	0.5	1.96	0.24
SG3 [11]	240	1154	20	814	135	1.80	60	0.45	1.95	0.24
SG4 [11]	309	1145	20	744	135	2.32	77	0.35	2.51	0.27
SG5 [11]	420	1121	20	698	140	2.80	47	0.3	2.80	0.30
SG6 [11]	168	1287	40	769	120	1.44	72	0.6	1.68	0.21
LG1 [11]	159	1496	80	625	102	1.36	68	0.45	1.59	0.18
WG1 [11]	159	1065	40	625	102	1.36	68	0.45	1.59	0.18
Roesler [12]	290	1107	19	718	160	1.68W.R+ 1.65F[1]	88	0.55	0.24	0.29
Einsfield [13]	420	992	9.5	860	149	11.5	S.P[2] 11.5	0.31	-	0.28
Casuccio G18 [14]	263	1080	30	835	184	-	-	0.7	1.5	0.27
Casuccio G37 [14]	431	1060	30	765	149	4.2	-	0.35	2.5	0.29
Casuccio G48 [14]	452	960	30	875	155	4.8	-	0.34	3.5	0.30
Zhang C40 [15]	397	1065	10,16, 20,25	532	205	-	70	0.52	-	0.36
Zhang C80 [15]	450	1144	10,16, 20,25	572	150	-	SF[3](50)	0.33	-	0.32

AE: Air entraining agent – [1] F is high range water reducer – [2] S.P is super plasticizer – [3] SF is silica fume.

Table 2: Beams dimensions.

Concrete	Beam	Height H [mm]	Width B [mm]	Span S mm	Notch /height a0/H	Mass [kg]	Concrete	Beam	Height H [mm]	Width B [mm]	Span S [mm]	Notch /height a0/H	Mass [kg]
C1	B1	150	80	600	0.33	16.53	**Zhang [15]**	all	100	100	400	0.1	9.2
	B2	150	70	600	0.37	15.71	**Casuccio**	all	105	75	400	0.5	~7.5
	B3	150	68	600	0.37	14.51	**SG3→6**	all	300	120	1200	0.4	~104
	B4	150	80	600	0.30	15.39	**WG1 [11]**	B1	250	120	1000	0.40	73.50
	B5	100	80	600	0.53	15.39		B2	300	120	1200	0.40	105.8
	B6	150	80	600	0.53	15.98		B3	400	120	1600	0.40	188.2
C2	B1	100	100	600	0.25	13.97	**LG1 [11]**	B1	400	240	1600	0.40	376.3
	B2	100	100	600	0.30	13.93		B2	450	240	1800	0.40	476.3
	B3	100	100	300	0.25	7.00		B3	500	240	2000	0.40	588.0
	B4	150	80	600	0.37	16.80		B4	550	240	2200	0.40	711.5
C3	B1	100	100	600	0.30	14.35	**SG1 [11]**	B1	300	120	1200	0.4	102.8
	B2	100	100	300	0.25	7.00		B2	400	120	1600	0.4	182.8
	B3	150	80	600	0.37	17.45	**Einsfeld [13]**	B1	76.2	38.1	400	0.50	7.43
Roesler [12]	**B1→3**	150	80	600	0.33	17.3		B2	152.4	38.1	400	0.50	7.56
	B4→6	250	80	1000	0.33	48		B3	304	38.1	400	0.50	7.69

3 Results and discussion

Table 3: Results of inverse analysis using bilinear softening curve.

Mix	Beam	Material properties			d_{max} [mm]	Paste volume [m^3/ m^3]	Size independent fracture parameters calculated from inverse analysis			
		F'c [MPa]	E [GPa]	Ft [MPa]			L_{ch} [mm]	W_1 [mm]	Wc [mm]	G_F [N/mm]
SG1	B1	43.8	31.4	3.73	20	0.24	763	0.038	0.510	0.332
	B2				20	0.24	744	0.036	0.518	0.329
SG3	B1	50.9	35.7	3.45	20	0.24	719	0.059	0.330	0.269
SG4	B1	56.4	35.9	3.67	20	0.27	688	0.056	0.299	0.258
SG5	B1	50.2	41	3.42	20	0.30	721	0.048	0.250	0.237
SG6	B1	50.8	38.9	3.45	40	0.21	872	0.030	0.370	0.262
WG1	B1	40	33.6	3.51	40	0.18	512	0.033	0.277	0.287
	B2				40	0.18	861	0.053	0.482	0.315
	B3				40	0.18	903	0.029	0.546	0.331
LG1	B1	40	33	3.51	80	0.18	1008	0.021	0.669	0.376
	B2				80	0.18	1037	0.028	0.635	0.387
	B3				80	0.18	1153	0.034	0.686	0.431
	B4				80	0.18	1058	0.031	0.645	0.395
C1	B1	33.7	35	3.70	20	0.28	540	0.069	0.220	0.211
	B2				20	0.28	530	0.065	0.216	0.208
	B3				20	0.28	473	0.041	0.191	0.185
	B4				20	0.28	523	0.040	0.178	0.204
	B5				20	0.28	480	0.046	0.232	0.188
	B6				20	0.28	507	0.045	0.250	0.198
Roesler	B1	58.3	32	3.74	20	0.29	455	0.027	0.280	0.195
	B2				20	0.29	489	0.033	0.301	0.214
	B3				20	0.29	426	0.020	0.201	0.186
	B4				20	0.29	555	0.034	0.375	0.242
	B5				20	0.29	372	0.024	0.200	0.163
	B6				20	0.29	354	0.023	0.172	0.155
C2	B1	50	46	5.15	20	0.29	284	0.015	0.169	0.163
	B2				20	0.29	238	0.012	0.135	0.137
	B3				20	0.29	296	0.028	0.153	0.172
	B4				20	0.29	201	0.009	0.155	0.116
C3	B1	33	31.12	3.33	20	0.29	717	0.040	0.340	0.256
	B2				20	0.29	722	0.041	0.430	0.257
	B3				20	0.29	566	0.008	0.324	0.223
R.Einsfield	B1	78	36.2	4.63	20	0.28	221	0.023	0.128	0.131
	B2				20	0.28	266	0.028	0.132	0.158
	B3				20	0.28	238	0.018	0.164	0.141
Casuccio	B1	18.1	27.1	3.40	30	0.27	247	0.014	0.194	0.106
	B2	37.5	33.1	4.10	30	0.29	259	0.015	0.175	0.132
	B3	48.4	39.9	5.30	30	0.30	164	0.010	0.171	0.136
Zhang C40	D10 B1	39.55	30	3.208	10	0.36	498	0.010	0.156	0.145
	D10 B2				10	0.36	373	0.015	0.106	0.135
	D16 B1	40.05	30	4.555	16	0.36	266	0.024	0.225	0.193
	D16 B2				16	0.36	253	0.014	0.227	0.177
	D20 B1	39.23	30	6.190	20	0.36	201	0.031	0.437	0.239
	D20 B2				20	0.36	200	0.019	0.374	0.219
	D25 B1	40.07	30	2.87	25	0.36	573	0.037	0.397	0.223
	D25 B2				25	0.36	834	0.055	0.433	0.217
Zhang C80	D10 B1	85.2	35	5.793	10	0.32	175	0.019	0.141	0.176
	D10 B2				10	0.32	195	0.026	0.168	0.199
	D16 B1	85.42	35	5.335	16	0.32	248	0.031	0.153	0.212
	D16 B2				16	0.32	197	0.025	0.155	0.172
	D20 B1	82.29	35	5.458	20	0.32	263	0.031	0.172	0.235
	D20 B2				20	0.32	263	0.031	0.172	0.235
	D25 B1	82.28	35	3.844	25	0.32	500	0.041	0.345	0.270
	D25 B2				25	0.32	633	0.042	0.293	0.232

All experimental data (experimental F-CMOD curves) of studied beams from different concretes were analyzed through the proposed inverse analysis procedure presented in section A.3 as described in Fig.A.3. This inverse analysis procedure has been put using MATALAB. In this procedure the size independent fracture parameters are calculated from minimizing the differences between numerical F-CMOD curve which is calculated from analytical model of Olesen (see appendix A.1), and experimental F-COMD curve obtained from three point bending test on notched beam. Fracture energy G_F and the characteristic length L_{ch} are determined using Eq.(A.3 and A.4) respectively. The results of inverse analysis as well as critical crack opening displacement w_c and kink point opening displacement w_1 are shown in Table 3.

In the following the relations between size independent fracture parameters from inverse analysis and materials properties of concrete are discussed.

3.1 The influence of compressive strength F'c on fracture energy G_F

The relation between G_F obtained from inverse analysis and $F'c^{0.7}$ is shown in Fig.1 It can be found that there is an increase in G_F when $F'c^{0.7}$ increases, while no clear and constant trend can be noticed with F'c.

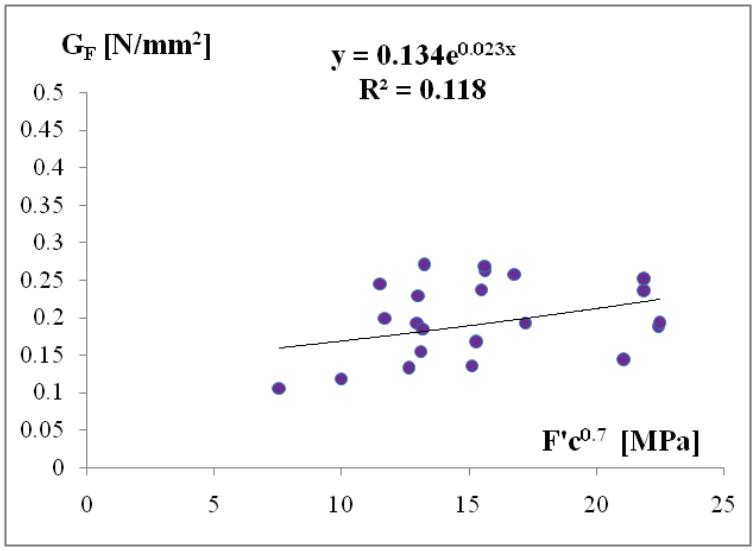

Figure 1: Fracture energy versus compressive strength.

Some researchers verified the relationship between fracture energy and compressive strength. Einsfeld [13], Xie et al [16] obtained average values for G_F that increase 13% and 11% for an increase of 53% and 29% in the compressive strength, respectively. Gettu et al. [17] compared the results obtained for high-strength concrete with conventional concrete. He verified that an increase of 160% in the compressive strength resulted in an increase of only 12% in the fracture energy. These results show the necessity of a relative great increase in the compressive strength in order to obtain a small increase in the fracture energy. Einsfield [13] has found that G_F decreases when F'c increases, (Einsfield studied concretes with F'c between 65 to 88 [Mpa] and d_{max}=9.5 [mm]), while Rao and Prasard [18] who studied concretes with F'c between 40 to 75 [Mpa] and d_{max}<20 [mm]) , Wu et al [19] and Gettu et al [17] (studied concretes with F'c >80 [Mpa] and d_{max}=9.5 [mm]) , found that G_F increases when F'c increases. Darwin [20] concluded that there is no clear relationship between G_F and F'c, (he studied concretes with F'c 20-99 [Mpa] and d_{max}=9, 12 [mm]). Other researches has found that G_F is not sensitive to F'c in high strength concrete [9]. The difference in the relationship between F'c and G_F in Normal Strength Concrete NSC and High Strenght Concrete HSC can be explained by the difference in the internal damage of concrete as cracks extend around aggregates in normal strength concrete but through aggregates in high strength concrete [8].

3.2 The effect of aggregates size on fracture properties

It can be shown from Table 3 that when the paste volume is fixed, G_F increases when the maximum aggregates size increases. For concrete mix LG1 and WG1, G_F increases 25% when d_{max} increases from 40 mm to 80 mm [11]. The same

trend was observed for Zhang beams too, as there was an increase about 30% in G_F when d_{max} increased from 10 to 25 [mm] for a fixed paste volume of 32%. It can also be noticed that when d_{max} increases the critical crack opening displacement, Wc, increases. For example, Wc increases from Wc = 0.42 [mm] for WG1 with d_{max} = 40 [mm] to Wc = 0.66 [mm] for LG1 with d_{max} = 80 [mm]. This can be noticed also in Zhang beams. In Fig.2 the variation of fracture energy with maximum aggregate size is plotted and an increase in frcture energy with the increase of aggregates size can be observed.

For a constant paste volume, the characteristic length, L_{ch}, increases when d_{max} increases as noticed from concretes WG1, LG1 and Zhang beams.

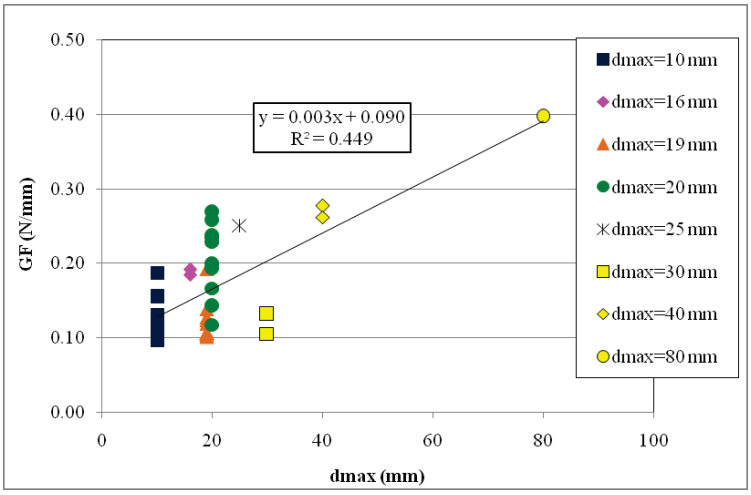

Figure 2: Fracture energy versus maximum aggregate size.

3.3 The effect of paste volume on fracture energy

Concrete consists of three phases: cement paste as matrix, interface transition zone, and aggregates. Each part has its own effect on fracture properties of concrete and consequently paste volume has an important role in fracture energy value. Paste volume is highlighted in this study and has been chosen instead of water to cement ratio w/c, because for the same w/c ratio we can make many concrete mixes with different F'c, for example when w/c=0.5 this may include an amount of cement about 300 Kg and 150 Liters of water, it can also include 400 Kg of cement with 200 Liters of water, so the w/c ratio does not take into account the cement content, while paste volume does. When paste volume increases the drying shrinkage increases too, consequently cracks increase and fracture energy decreases [21, 22].

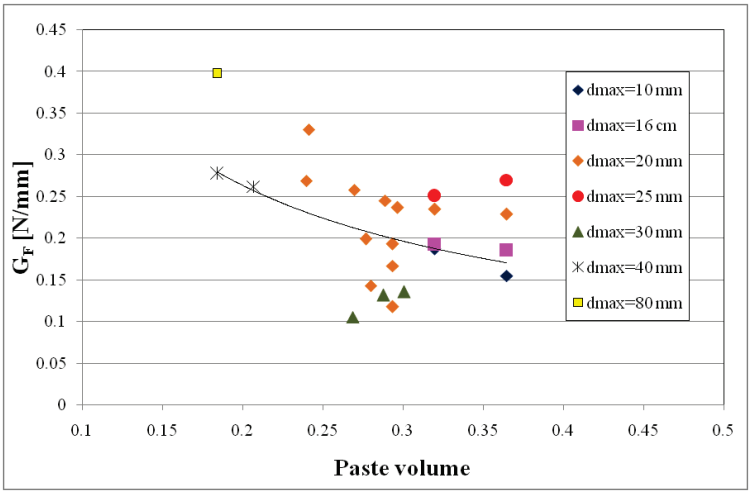

Figure 3: The relation between G_F and paste volume.

In this research the statistical studies has shown a better trend between paste volume and fracture energy as shown in

Fig.3 more than the trend with w/c ratio. From this figure it can be remarked that GF decreases with the increase of paste volume. Similar observations have been found by Roziere et al. [22] who found by acoustic emission test that the width of FPZ decreases with the increase in paste volume and this explains the decrease in GF with the increase in paste volume.

The relation of characteristic length with paste volume is plotted in Fig.4. The results show that the characteristic length is affected by paste volume more than the maximum aggregate size. The length of the fracture process zone at crack growth is approximately proportional to characteristic length which is a pure material property [1]. Hence, the decrease in characteristic length indicates the decrease in FPZ width.

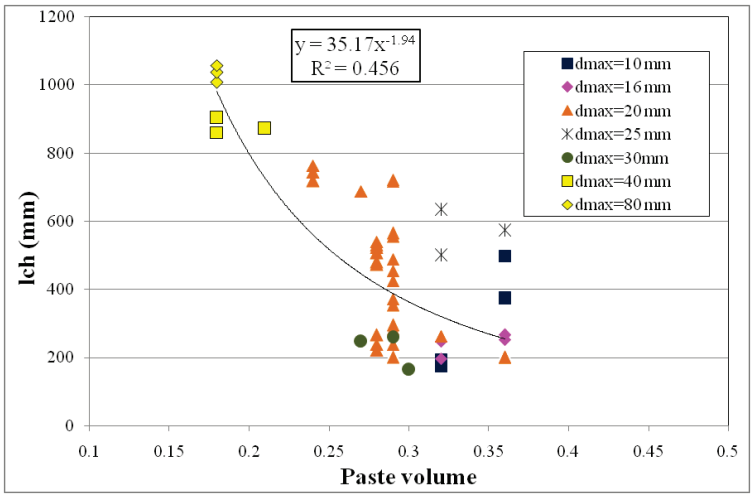

Figure 4: Variation of characteristic length with paste volume.

3.4 New empirical relation for G_F:

Empirical relations for G_F were presented in the literature using F'c, d_{max} [10], others used water to cement ratio [8]. Fracture energy, G_F, may be computed using the empirical equation proposed by "Comité Euro-International du Béton" (CEB) [10].

$$G_{F(CEB)} = \alpha_d . (\frac{F_c'}{10})^{0.7} \quad (1)$$

Where α_d is a coefficient related to d_{max} and equal to 0.025, 0.03, 0.058 when d_{max} equal to 8, 16, 32. G_F is given in [N/mm] and F'c in [MPa]. The calculated values using inverse analysis procedure are close from the predicted values using Eq. 1, (Fig.5) where a difference about 35% is found. Indeed, this difference is explained by the size dependant data used initially to fit this equation, and the negligence of paste volume as a key parameter. However, the predicted values may be considered as the lower bounds of the true fracture energy values.

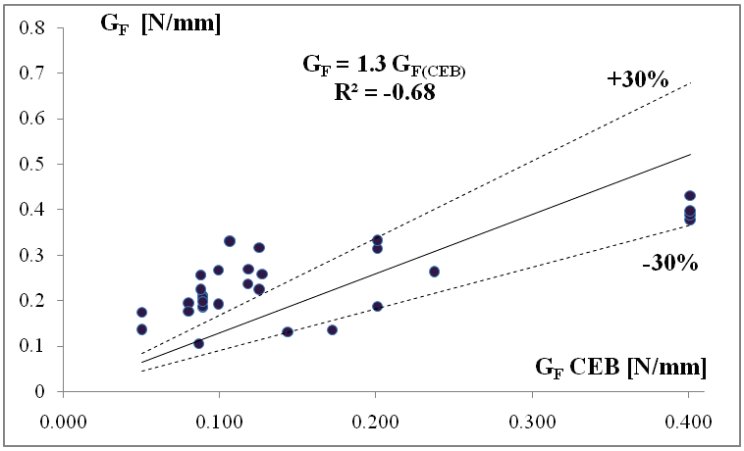

Figure 5: Variation of fracture energy with compressive strength and aggregate size.

Bazant and Becq-Giraudon [8] have proposed the following empirical relation for G_F depending on d_{max}, F'c, water to cement ratio w/c, and aggregate type.

$$G_{F(\text{Bazant})} = 2.5\alpha_0 \left(\frac{F'_c}{0.051}\right)^{0.46} \left(1 + \frac{d_{max}}{11.27}\right)^{0.22} \left(\frac{w}{c}\right)^{-0.30} \quad (2)$$

Where: α_0=1 for rounded aggregates, α_0=1.44 crushed or angular aggregates. F'c is in [MPa], d_{max} is in [mm] and G_F is in [N/m]. Bazant and Becq-Giraudon [8] used different types of tests and different sizes of specimen therefore the predicted results are far from the intrinsic fracture energy calculated by inverse analysis (Fig.6).

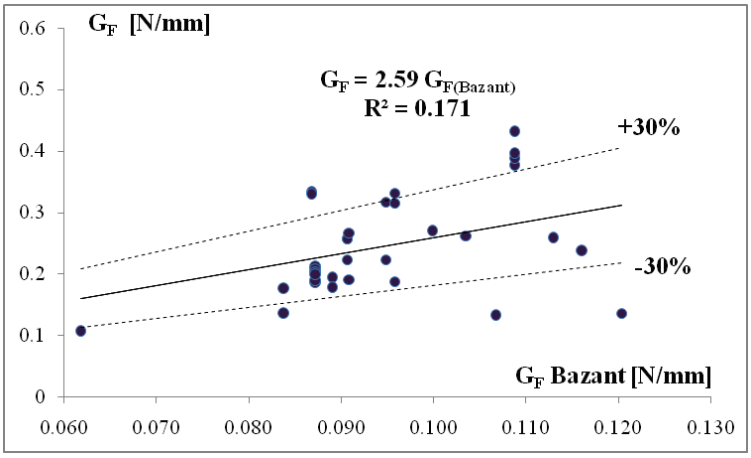

Figure 6: Variation of fracture energy with compressive strength, aggregate size and W/C ratio.

Based on the obtained results (Fig.2 and Fig.3), a new empirical relation is presented using size independent G_F depending on linear regression. This relation is similar to Bazant's but depends on paste volume instead of w/c ratio adding to F'c and d_{max}. The relation is:

$$G_F = F'^{0.7}_c \left[0.003\left(1 + \frac{d_{max}}{10}\right) + P_V^{5.7}\right] \quad (3)$$

Where P_v is the paste volume given in [m^3/m^3], F'c in [MPa], d_{max} in [mm], and G_F in [N/mm]. The parameters were searched using excel solver, with a tolerance equals to 5%, a convergence equals to 0.0001, and the research was done using Newton option. The comparison between the predicted G_F using Eq.(3) and the calculated G_F is shown in Fig.7. It can be concluded that this new model can be regarded as a method to predict fracture energy of all grades of concrete from their compressive strength, maximum aggregate size and paste volume.

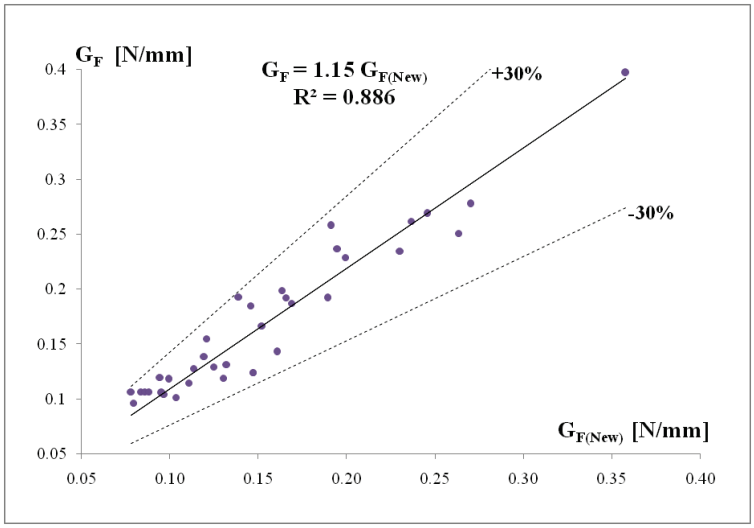

Figure 7: The predicted fracture energy GF versus calculated one.

3.5 Generalized bilinear curve

For the sake of searching a generalized bilinear softening curve, the average bilinear softening curve of each d_{max} has been found and plotted as shown in Fig.8. The comparison between generalized bilinear curves of the present work with other bilinear cuves of Wittmann [2] , RILEM [3], CEB [10] is detailed in Table 4.

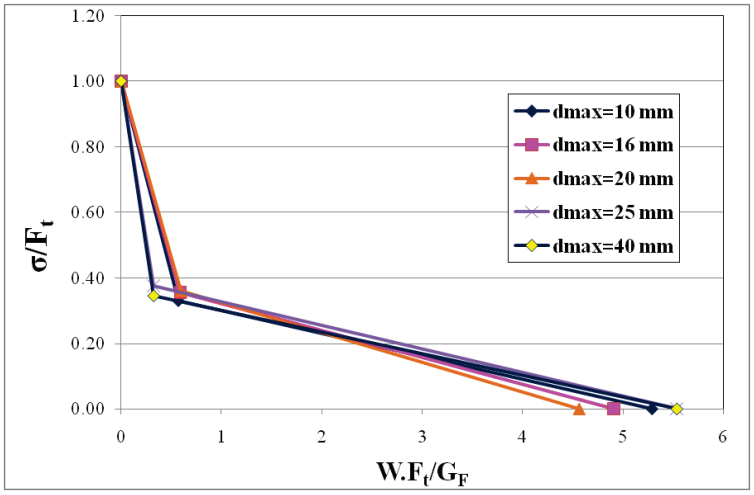

Figure 8: Average bilinear curves for different d_{max}.

From Fig.8 it can be noticed that the strength at the kink point does not depend on the aggregate size. The mean value of the strength at the kink point is 0.35Ft which is close to RILEM one which is Ft/3 but not very far from Wittmann one which is 0.25Ft. It can also be remarked that w_1 differs due to d_{max} that affects on wc too. The relation between $w_1.F_t/G_F$ and $w_c.F_t/G_F$ has been plotted as a function of d_{max}, see Fig.9. The following relation for W_1 has been found:

$$w_1 = \frac{1.4G_F}{F_t} - w_c \tag{4}$$

It can be seen on Fig.9 that points of d_{max} 10, 40, 80 [mm] are far from the line, which means that the relation of w_1 is more precise for the medium d_{max} within the range 16 to 30 [mm] than small and large d_{max}. CEB [10] gives the relation $W_c=\alpha G_F/F_t$ where α is a coefficient depends on dmax. In the present work The values of α is 5.043, see Fig.10, which is almost the same value of Wittmann taken equal to 5.

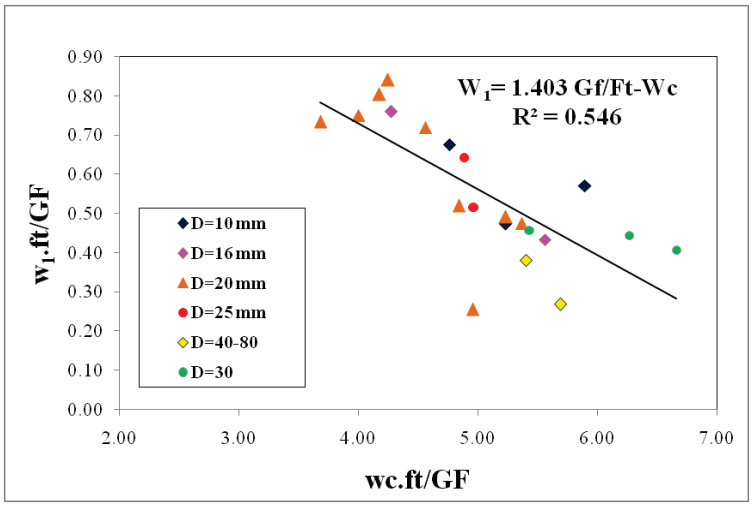

Figure 9: The relation between W_1 and Wc, F_t, G_F for different d_{max}.

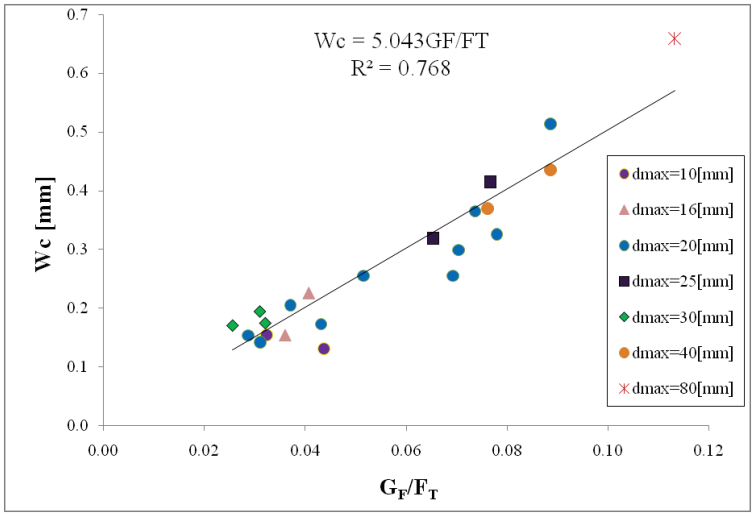

Figure 10: The relation between Wc and G_F/F_T.

Table 4: The generalized bilinear curve coordinates.

	RILEM	**Wittmann**	**CEB**	**Present work**
W_1	$0.8G_F/F_t$	$0.75G_F/F_t$	$2G_F/F_t$ -0.15W_c	$W_1=1.4G_F/F_t$ -W_c
W_c	$3.6G_F/F_t$	$5G_F/F_t$	$\alpha.G_F/F_t$	$5G_F/F_t$
Kink point strength	F_t /3	0.25 F_t	0.15 F_t	0.35 F_t

4 Conclusion

Size independent fracture parameters including bilinear softening curve were found using inverse analysis approach based on the fictitious crack model and the analytical bilinear softening model. The analysis of the obtained size independent parameters showed that fracture energy is affected by compressive strength F'c, maximum aggregate size d_{max}, paste volume. A new empirical relation for predicting G_F in concrete was presented using F'c, d_{max}, and paste volume. Generalized bilinear softening curves from inverse analysis were derived and compared with generalized bilinear curves found in the literature. The results were close to Wittmann generalized bilinear curve but far from CEB one.

Appendix A. Analytical Hinge Model

The crack propagation in beams loaded in bending may be modeled analytically using the non linear hinge model developed firstly by Ulfkjaer [5], who depended on linear softening, and improved later by Olesen [6], who depended on bilinear softening. The model provides an analytical solution for calculating the numerical Force - Crack Mouth Opening Displacement (F-CMOD) curve. The area around the crack is modeled as an array of elastic layers within it, the strain-softening takes place, while outside it, the behavior of the studied element remains elastic. The constitutive behavior law for each layer is assumed to be linear elastic in the pre-crack state, while the cracked state is approximated by a bilinear σ-w softening relationship [2, 6]. The stresses are controlled by Eq.(A.1)

$$\sigma = \begin{cases} \sigma(\varepsilon) = E.\varepsilon & \text{Pre-cracked state} \\ \sigma_w(w) = g(w).f_t & \text{Cracked state} \end{cases} \qquad \text{(A. 1)}$$

Where E is the elastic modulus, ε: the elastic strain, $\sigma_w(w)$: the stress-crack opening relationship where w: crack opening, f_t: the uni-axial tensile strength. The function g(w) is defined mathematically by the expression (Fig.A.1):

$$g(w) = b_i - a_i w = \begin{cases} b_1 - a_1 w & 0 \le w < w_1 \\ b_2 - a_2 w & w_1 \le w \le w_c \end{cases} \quad \text{(A. 2)}$$

Where: $b_1 = 1$, $w_1 = \dfrac{1-b_2}{a_1 - a_2}$, $w_c = \dfrac{b_2}{a_2}$.

Fracture energy, $G_{F,}$ is given by the equation

$$G_F = \frac{f_t}{2}(w_1 + b_2(w_c - w_1)) \quad \text{(A. 3)}$$

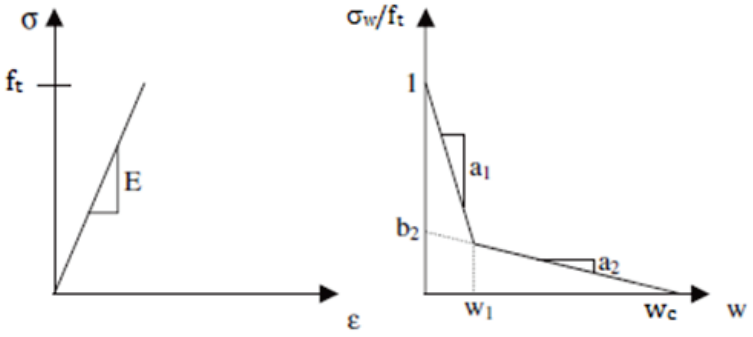

Figure A. 1: stress-strain relationship for pre-cracked state and cracked state.

The characteristic length is expressed by the relation

$$l_{ch} = \frac{E.G_F}{f_t^2} \quad \text{(A. 4)}$$

The hinge model geometry and the stress distribution are presented in Fig.A.2. The span is given by L and the beam's width by b.

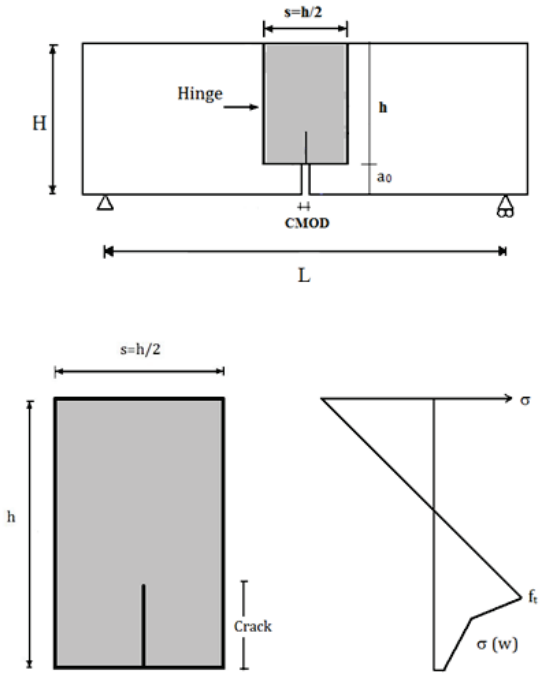

Figure A. 2: Hinge geometry and stress distribution.

A.1. Static equilibrium of the hinge

The fracture process is divided into four phases. Phase I is the linear one, where no cracks are formed while phase II is the linear cracking, phase III is the bilinear cracking and phase IV is the bilinear cracking with propagation [6]. For the sake of simplicity, the hinge solution is presented in terms of normalized properties where the following dimensionless variables are used:

$$\beta_1 = \frac{f_t a_1 s}{E},\ \beta_2 = \frac{f_t a_2 s}{E},\ c = \frac{(1-b_2)(1-\beta_1)}{\beta_2 - \beta_1} \tag{A. 5}$$

$$\mu = \frac{6M}{f_t b h^2},\ \theta = \frac{hE\varphi}{sf_t},\ \alpha = \frac{d}{h} \tag{A. 6}$$

Where M is the bending moment, φ is the rotation and d is the crack length. The solution for all phases gives the normalized bending moment μ and the normalized crack length α as functions of the normalized rotation θ. The behavior of the hinge is described by following equations:

Phase I: $0 < \theta \le 1$

The pre-cracked behavior of the hinge is expressed by

$$\alpha = 0 \text{ and } \mu = \theta \tag{A. 7}$$

Phase II: $1 < \theta \le \theta_{I-II}$

$$\alpha = 1 - \beta_1 - \sqrt{(1-\beta_1)(\frac{1}{\theta} - \beta_1)} \tag{A. 8}$$

$$\mu = 4(1 - 3\alpha + 3\alpha^2 - \frac{\alpha^3}{1-\beta_1}) \tag{A. 9}$$

With $\theta_{I-II} = 0.5(1 - c + \sqrt{(1-c)^2 + \frac{c^2}{\beta_1 - 1}})$

Phase III: $\theta_{I-II} < \theta \le \theta_{II-III}$

$$\alpha = 1 - \beta_2 - \frac{1-b_2}{4\theta}(2-\beta_2) - \sqrt{(1-\beta_2)\frac{(2-\beta_2)(1-b_2)^2}{(4\theta)^2(1-\beta_2)} - \beta_2 + \frac{(1-b_2)\beta_2}{2\theta} + \frac{b_2}{\theta}} \tag{A. 10}$$

$$\mu = 4(1 - 3\alpha + 3\alpha^2 - \frac{\alpha^3}{1-\beta_2})\theta + (6\alpha - 3) - \frac{(1-b_2)(3-\beta_2)\alpha^2}{1-\beta_2} \tag{A. 11}$$

With $\theta_{II-III} = 0.5(\frac{b_2}{\beta_2} + \sqrt{\frac{\beta_2}{4}(1-b_2)^2 + \frac{1}{2}(1-b_2^2) + \frac{b_2^2}{\beta_2}})$

Phase IV: $\theta > \theta_{II-III}$

$$\alpha = 1 - \frac{1}{2\theta}(1 + \sqrt{1 - b_2 + \frac{b_2^2}{\beta_2}}) \tag{A. 12}$$

$$\mu = 4(1 - 3\alpha + 3\alpha^2 - \alpha^3)\theta + (6\alpha - 3) - 3\alpha^2 + \frac{b_2}{4\theta^2}(1 - \frac{b_2}{\beta_2})^2 - \frac{b_2(1-\alpha)}{2\theta}(1 - \frac{b_2}{\beta_2}) \tag{A. 13}$$

The bending moment is given by the equation:

$$M = \frac{PL}{4} + \frac{m_b.g.L}{8} \tag{A. 14}$$

Where P is the load and m_b is weight of the beam in span. From the knowledge of normalized moment μ and using Eq.(A.14) the force can be calculated through the following equation

$$P = \frac{2\mu f_t h^2 b}{3L} - \frac{1}{2} m_b.g \tag{A. 15}$$

A.2. Crack Mouth Opening Displacement (CMOD)

CMOD is defined as the opening of the crack at a distance from the crack mouth located at d_0 and it depends on three different contributions as the following:

$$CMOD = COD + COD_g + COD_e \tag{A. 16}$$

The first term is COD related to the crack opening and is given by:

$$COD = \frac{sf_t}{E} \frac{1 - b_i + 2\alpha\theta}{1 - \beta_i} \tag{A. 17}$$

Where $(b_i, \beta_i) = \begin{cases} (1, \beta_1) & Phase \quad II \\ (b_2, \beta_2) & Phase \quad III \\ (0,0) & Phase \quad IV \end{cases}$

The second term COD_g is the geometrical opening due to the distance from the notch tip to the measurement point and is expressed by the following equation given by Stang [23]:

$$COD_g = \frac{sf_t 2(a_0 + d)}{hE}(\theta - 1) \tag{A. 18}$$

The third term COD_e is the elastic deformation of the specimen and may be evaluated using the following equation [7]:

$$COD_e = \frac{6PLa_0}{EbH^2} \upsilon_1 \tag{A. 19}$$

υ_1 is a geometrical function where its best value is the mean of tow expressions given by Stang [23] and Karihaloo [24]. According to Stang υ_1 is given by Eq.(A.20).

$$\upsilon_1 = (\frac{a_0 + d}{a_0})(0.76 - 2.28x + 3.87x^2 - 2.04x^3 + \frac{0.66}{(1-x)^2}) \tag{A. 20}$$

Where: $x = \frac{a_0}{H}$.

According to Karihaloo υ_1 is expressed by the expression:

$$\upsilon_1 = 0.76 - 2.28y + 3.87y^2 - 2.04y^3 + \frac{0.66}{(1-y)^2} \tag{A. 21}$$

With: $y = \frac{a_0 + d}{H + d}$

Using Eq. (A.15 and A.16) the analytical Force-CMOD curve may be evaluated.

A.3. Determining of bilinear σ-w relationship by inverse analysis

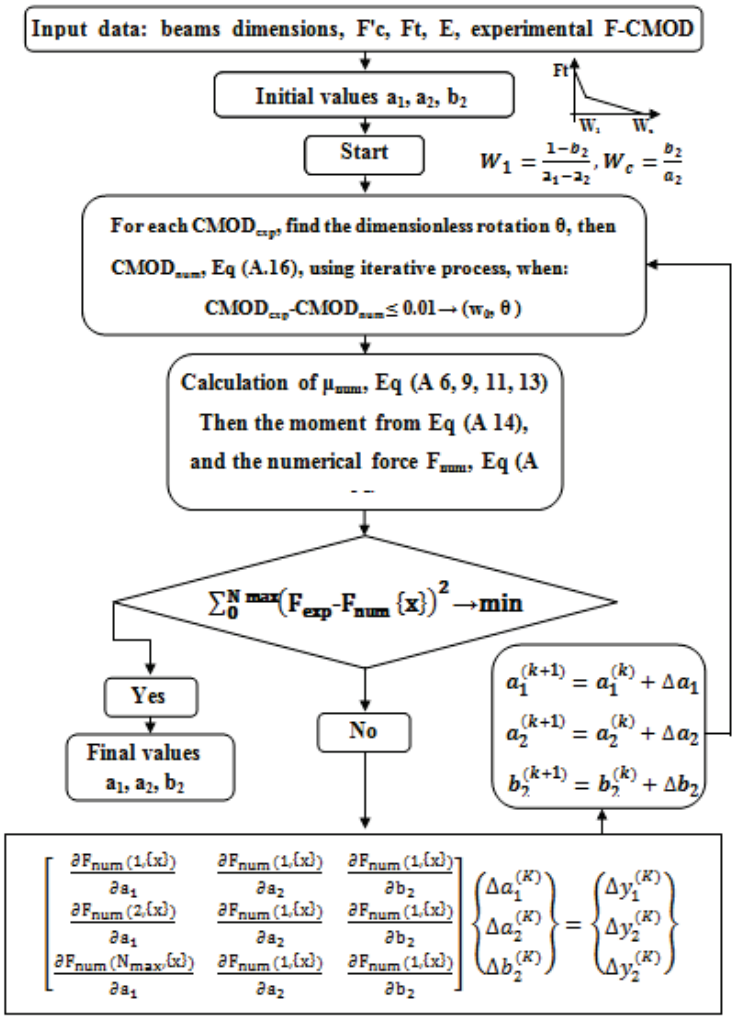

Figure A. 3: Flow chart of inverse analysis procedure using bilinear softening curve.

Inverse analysis procedure aims to get the size independent fracture energy and the parameters of strain-softening curve [2, 7]. This can be achieved by minimizing the square differences between experimental and numerical F-CMOD curves, where the experimental curve is derived from three points bending test on notched beam, and the numerical one is calculated from the analytical model of Olesen, where the shape of the σ-w relationship is bilinear, and its parameters are shown in Fig.A.1.

The input data are the experimental F-CMOD curve, the concrete properties (E, F_t), the beam dimensions and the initial values for a_1, a_2, b_2. Through an iterative process, each parameter is searched by minimizing the difference between experimental and numerical F-CMOD curves (Fig.A.3). The process is stopped when the relative difference between two sequences of optimization is less than 1%. The output data of inverse analysis procedure are: the fracture energy, the characteristic length, and the parameters of bilinear softening curve a_1, a_2, b_2. The inverse analysis procedure is considered validate if the standard deviation of G_F from the same concrete is less than 10% [2, 7]. As all standard deviations of fracture energy and other output parameters are less than 10% for the same concrete in this work, then the inverse analysis procedure is considered validate.

This step-by-step inverse method has many advantages. In fact, it is simple and precise and the individual optimization of parameters has no local minimization problem, as those encountered in the case of global optimization of all variables in one minimization step.

REFERENCES

[1]- A. Hillerborg, M. Modéer, P.-E. Petersson, Analysis of crack formation and crack growth in concrete by means of fracture mechanics and finite elements. Cement Concrete Res., 6(6) (1976) 773-781.

[2]- F.H. Wittmann, K. Rokubo, E. Brühwiler, H. Mihashi, P. Simonin, Fracture energy and strain softening of concrete as determined by means of compact tension specimens, Mater. Struct. 21(1) (1988) 21-32.

[3]- Rilem 50-FMC Draft Recommendation, Determination of the fracture energy of mortar and concrete by means of three-point bend tests on notched beams. Mater. Struct. 18(4) (1985) 287-290.

[4]- K. Duan, X.-Z. Hu, F.H. Wittmann, Size effect on fracture resistance and fracture energy of concrete, Mater. Struct., 36(2) (2003) 74-80.

[5]- J.P. Ulfkjaer, S. Krenk, R. Brincker, Analytical Model for Fictitious Crack Propagation in Concrete Beams. J. Eng. Mech.-ASCE, 121(1) (1995) 7-15.

[6]- J.F. Olesen, Fictitious Crack Propagation in Fiber-Reinforced Concrete Beams. J. Eng. Mech.-ASCE, 127(3) (2001) 272-280.

[7]- L. Ostergaard, Early-Age Fracture Mechanics And Cracking of Concrete. Experiments and Modelling, PhD Thesis, Department of Civil Engineering, Technical University of Denmark, 2003.

[8]- Z.P. Bazant, E. Becq-Giraudon, Statistical prediction of fracture parameters of concrete and implications for choice of testing standard. Cement Concrete Res., 32(4) (2002) 529–556.

[9]- Z. Dong, W. Keru, Fracture Properties of High-Strength Concrete, doi:10.1061/(ASCE)0899-1561(2001)13:1(86), J. Mater. Civil Eng., 13(1) (2001) 86-88.

[10]- Comité Euro-international du Béton - Fédération Internationale du Béton : CEB-FIP Model Code 1990 : Design Code, Ed. Thomas Telford, 1993.

[11]- Z. Zhao, S.H. Kwon, S.P. Shah, Effect of specimen size on fracture energy and softening curve of concrete: Part I. Experiments and fracture energy. Cement Concrete Res., 38(8-9) (2008) 1049-1060.

[12]- J. Roesler, G.H. Paulino, K. Park, C. Gaedicke, Concrete fracture prediction using bilinear softening. Cement and Concrete Comp., 29(4) (2007) 300-312.

[13]- R.A. Einsfeld, M.S.L. Velasco, Fracture parameters for high-performance concrete. Cement Concrete Res., 36(3) (2006) 576-583.

[14]- M. Casuccio, M.C. Torrijos, G. Giaccio, R. Zerbino, Failure mechanism of recycled aggregate concrete. Constr. Build. Mater., 22(7) (2008) 1500-1506.

[15]- J. Zhang, C.K.Y. Leung, S. Xu, Evaluation of fracture parameters of concrete from bending test using inverse analysis approach, Mater. Struct., 43(6) (2010) 857-874.

[16]- J. Xie, A.E. Elwi, J.G. MacGregor, Mechanical Properties of Three High-Strength Concretes Containing Silica Fume. ACI Mater. J., 92(2) (1995) 135-145.

[17]- R. Gettu, Z.P. Bazant, M.E. Karr, Fracture Properties and Brittleness of High-Strength Concrete. ACI Mater. J., 87(6) (1990) 608-618.

[18]- G.A. Rao, B.K.R. Prasad, Fracture energy and softening behavior of high-strength concrete. Cement Concrete Res., 32(2) (2002) 247-252.

[19]- K.-R. Wu, B. Chen, W. Yao, D. Zhong, Effect of coarse aggregate type on mechanical properties of high-performance concrete. Cement Concrete Res., 31(10) (2001) 1421-1425.

[20]- D. Darwin, S. Barham, R. Kozul, S. Luan, Fracture Energy of High-Strength Concrete. ACI Mater. J., 98(5) (2001) 410-417.

[21]- F.E. Amparano, Y. Xi, Y.-S. Roh, Experimental study on the effect of aggregate content on fracture behavior of concrete. Eng. Fract. Mech., 67(1) (2000) 65-84.

[22]- E. Rozière, S. Granger, Ph. Turcry, A. Loukili, Influence of paste volume on shrinkage cracking and fracture properties of self-compacting concrete. Cement and Concrete Comp., 29(8) (2007) 626-636.

[23]- H. Stang, Analysis of 3 points bending test, Technical Report EU Contract - BRPR - CT98 - 813, Report from Test and Design Methods for Steel Fibre Reinforced concrete. 2000.

[24]- B.L. Karihaloo, P. Nallathambi, Notched beams test: mode I fracture toughness, in Fracture Mechanics Test Method for concrete, S. Shah and A. Carpiteri, Editors., Chapmann & Hall. chapter 1, (1991) 1-86.